Very Long Baseline Interferometry Covariance

J. W. Layland
Communications Systems Research Section

This article summarizes the methods and results of a covariance calculation for determination of DSN station location and clock parameters using very long baseline interferometry (VLBI) observation of Quasars. Errors of observation are assumed to arise from random (thermal) noise at the receiving antenna, and from errors in modeling the tropospheric delay. The critical error source is seen to be the troposphere: If errors in troposphere modeling are uncorrelated between observations, then 30–50 cm station-location determinations can be obtained with current modeling accuracies; if, however, these errors are correlated, then a factor-of-ten improvement in prediction of the tropospheric delay is needed to achieve this accuracy range.

I. Introduction

This article summarizes the methods and results of a covariance calculation for determination of DSN station location and clock parameters using VLBI observation of Quasars. A given observation set may currently include up to five stations and ten radio sources. Unknown parameters assumed to be simultaneously solved include the three-dimensional station location, two station clock parameters and the location of the Quasars. Both time delay and fringe frequency are observed. Errors of observation are assumed to arise from random (thermal) noise at the receiving antenna and from errors in modeling the tropospheric delay. The critical error source is seen to be the troposphere: If errors in troposphere modeling are uncorrelated between observations, then 30–50 cm station-location determinations can be obtained with current modeling accuracies; if, however, these errors are correlated, then a factor-of-ten improvement in prediction of the tropospheric delay is needed to achieve this accuracy range. Thermal noise, which is independent between observations, is comparatively insignificant relative to current troposphere errors if sufficient data are recorded for reliable detection of each Quasar (10^6 to 10^7 bits per observation).

II. Problem Model

The radio stars are located in space by their right ascension (RA) (α) and declination (dec) (δ). Tracking

stations are assumed to lie on the surface of a spherical Earth, and are hence also located by their α and δ coordinates and by a third coordinate, ρ, representing local variations from the mean Earth radius. (The geometry of the problem is described in Ref. 1.) Station clock offsets and clock rate offsets are assumed to be nominally zero but are treated as solved-for parameters in the covariance calculation. An observation is possible whenever any radio star is simultaneously in view of two or more of the tracking stations. A radio star is in view of a station whenever its elevation angle at that station is above some prespecified limit value. An observation set consists of a 24-hour interval during which the set of stars to be observed is rotated through the sky in steps of (typically) $\pi/100$ radians. At each step, any observation which is possible is added to the data set. No attempt is currently made to optimize the observing pattern or to eliminate conflicts in station usage. Some observations may occur simultaneously at three or more stations if their locations permit. The number of stations and their locations, and the number of stars and *their* locations are all variable data parameters. Most of the calculations to be described in the following have been performed using the three DSN stations at Goldstone, Calif., Canberra, Australia, and Madrid, Spain, for which no three-station observations are possible.

A VLBI observation results in noisy estimates of the time delay and doppler frequency difference between the observed Quasar noise signals at the two stations. Errors in the observation arise from thermal noise, from errors in modeling the propagation medium, and various other causes not to be considered here. Earth's troposphere consists of a thin shell over its surface. At Zenith elevation angle, this shell adds approximately 2 meters of additional delay to the path of a radio signal. As the elevation is lowered, the signal path travels through an increasingly longer segment of this tropospheric shell. If we let $\Delta\rho_z$ be the standard deviation of the error in modeling the tropospheric delay at zenith, and assume that this modeling error scales as the length of the in-troposphere signal path, then the standard deviation of the tropospheric delay model error at an elevation γ is

$$\Delta\rho_r = \Delta\rho_z/[A + \sin(\gamma)] \quad (1)$$

approximately, where $A \approx 0.02$. Furthermore, if we assume that any given observation is taken through a zone of troposphere which is reasonably layered and static, then the frequency error induced into the measurement results directly from Earth rotation, and changes in γ.

$$(d/dt)(\Delta\rho_r) = -\Delta\rho_z \cos\gamma \times (d/dt)(\gamma)/[A + \sin\gamma]^2 \quad (2)$$

The frequency error inferred in this way is clearly correlated with the delay error. Nothing in this formulation prevents us from assuming that different observations are taken through different zones of troposphere, and hence that the tropospheric modeling errors for each observation are independent. Current modeling capability is believed to be accurate to about 3% (Ref. 2), giving us

$$\Delta\rho_z \approx 2 \times 10^{-10} \text{ sec} \quad (3)$$

using only surface weather measurements at the tracking stations. It is expected that this figure can be reduced by a factor of 3–5 by using water vapor radiometer calibrations.

The effect of thermal noise depends upon the amount of data recorded and the time-and-frequency space spanned by the data-taking operation. Let us suppose that the spanned bandwidth of an observation is 20 MHz and the spanned time is 200 seconds. Suppose further that enough data are recorded to achieve a 6% resolution of the resultant ambiguity function; this can, for example, be achieved with 10^6 recorded bits from a 0.5 flux-unit ratio source observed by two 64-m antennas (Ref. 3). With this strategy, the standard deviation of the time delay measurement error is

$$\Delta\tau \approx 3 \times 10^{-9} \text{ sec} \quad (4)$$

Likewise, the frequency measurement error is $\Delta\nu_F = 3 \times 10^{-4}$ Hz. Assuming an S-band center frequency, and scaling by the Earth rotation rate for numerical convenience, we define

$$\Delta D \equiv \Delta\dot{\tau}/\omega_e \approx 2 \times 10^{-9} \text{ sec} \quad (5)$$

The three parameters $\Delta\rho_z$, $\Delta\tau$, and ΔD are variable data for the covariance calculations, with nominal values given by Eqs. (3)–(5). For any observation, the standard deviation of the error of observation is the rms of the thermal noise of the observation, and the tropospheric model error at each of the two stations. In the covariance calculation, all observations may be equally weighted, or weighted by the reciprocal of their variance. More sophisticated weightings dependent upon the errors projected into station locations could presumably improve the results.

Although the observed parameters are the Quasar noise signal time delay and doppler, the parameters of interest are the geometrical station and star locations. The time delay and doppler at a station, S_r relative to a fictional

station at the Geo-Center, are defined in terms of the observing geometry by the two nonlinear equations:

$$\tau = Z_r \sin \delta + r_r \cos \delta \cos (\alpha_r - \alpha) + C_r + \dot{C}_r \alpha_r \quad (6)$$

$$D = -r_r \cos \delta \sin (\alpha_r - \alpha) + \dot{C}_r \quad (7)$$

where (α, δ) are the Quasar RA and dec, (α_r, r_r, Z_r) the cylindrical coordinates of S_r at the time of observation, and C_r and $\dot{C}_r$ are the station clock offset and clock rate offset. Using R_e as the mean Earth radius, $Z_r = R_e (\rho_r \sin \delta_r)$ is the projection of the station position on Earth's spin axis, and $r_r = R_e \rho_r \cos \delta_r$ is its spin radius, or the projection on the equatorial plane, where $(\alpha_r, \delta_r, \rho_r)$ are the previously defined spherical coordinates of S_r. The observed time delay and doppler are of course the differences between the geocentric delays and dopplers at two observing stations.

The parameters of interest are derived from the observed parameters through a nonlinear least-squares estimation procedure. Details of such procedures in a radar context may be found in Ref. 4. The parameters to be solved for are station locations, rather than baselines, for ease in handling multiple baseline data. One real station, usually Goldstone, is used as reference for station coordinates, and one Quasar RA is also used as reference. The solution is assumed to be performed in a cylindrical coordinate system. The covariance of the errors resulting from the nonlinear least-squares estimation procedure is estimated by pretending that the problem is linear in the neighborhood of the solution point and applying the covariance result for a linear least-squares problem.

III. Summary of Calculations and Results

The first set of calculations, shown in Fig. 1, was intended to provide some direct comparison with the published results of Thomas and Fanselow (Ref. 5). These calculations do not include tropospheric errors. Two difficulties arise with this comparison. First, the coordinate systems used are not identical, so direct vector comparison is not convenient, although rss error-length comparison is. Second, the shape and size of the location error pattern has been observed to be a very strong function of the observation strategy. The observation set of Ref. 5 was at least partially optimized, whereas the observation set used here was wholly naive. The rss of the Madrid location error is shown in Fig. 1 for two observation sets for $\Delta\tau = 1 \times 10^{-9}$ second, and various ΔD. Other values of $\Delta\tau$ can be determined by appropriate scaling of both $\Delta\tau$ and ΔD. The poorer of the two observation sets shown consists of 118 observations of three stars located at (RA, dec) = (0., 0.8), (1., -0.05), (2.2, 0.1). The better observation set consists of 95 observations of these same three stars, plus 5 observations of a star located at (1.3, 1.5). The Madrid location error for both of these sets is noticeably poorer, with larger doppler errors than the Goldstone–Madrid rss baseline error as estimated from the results reported in Ref. 5. I believe at this time that this difference results wholly from the comparison difficulties cited above, principally the difference in observation strategy.

The remainder of the calculated errors to be presented include tropospheric effects, and most are computed at the nominal parameter values of Eqs. (3)–(5). For each calculated experiment, only the largest vector component of the station location error set is graphed; in most cases, this largest component is the Z-projection of the Canberra, Australia, station.

Figure 2 shows the one-sigma station location errors for a VLBI experiment involving the three DSN 64-meter stations and three radio stars at declinations of 0 and ±0.55 rn. The lower set of curves shows the expected resultant station location error for this particular experiment set. The upper set of curves shows the station location error scaled by the square root of the number of observations, which itself varies with elevation angle. This serves as a figure-of-merit for the observation pattern, and also indicates crudely what the deterioration in results would be if the errors of observation were correlated rather than independent. The improvement in results by weighting of the input data is also clear from this figure.

Some very low-elevation observations result in dramatic reduction of the location error indicated in Fig. 2. Upon inspection, it appears that these critical observations are the very few observations possible on the improbably long Madrid–Canberra baseline. With the exception of these observations, the best elevation limit would appear to be in the neighborhood of 10 to 12 degrees, and perhaps such a limit is appropriate on baselines with better visibility, with observations made at 3 to 4 degrees on the Madrid–Canberra baseline only.

Figure 3 is another look at the Canberra declination error for a VLBI experiment involving the three DSN 64-meter stations and three radio stars at declinations of 0 and ±0.35 rn. This smaller declination spread allows observations to be made on the Canberra–Madrid baseline at slightly higher elevations, which is, in turn, reflected in a different signature for location error vs. elevation. The

decreased spread in declination of the stars results in some decrease in the attainable station location resolution.

Looking at Fig. 2, there is some temptation to believe that the observations at or near the horizon are the most important to reducing the station location errors. Accordingly, a covariance calculation was performed which limited the elevation angle of at least one station of the pair to a band within 10 degrees of the selected horizon. This is shown in Fig. 4 for the same data as in Fig. 2. At best, only a slight benefit has accrued from this strategy at the higher horizon limit values, and a sizeable loss has accrued for low horizon limits.

Figure 5 shows the Canberra Z error obtained when the observations are perturbed by the tropospheric modeling error only. As in Fig. 2, the stars are located at 0 and ±0.55 rn. This approximates the situation obtained when a very large amount of data is recorded for each observation. The dependence upon the very low-elevation observations is enhanced in this figure.

There is at least an academic interest in knowing what improvements can be achieved by using additional tracking stations. This has been investigated for specific additions, with the results shown in Figs. 6 and 7. The stars observed are at declinations of 0 and ±0.55 rn. Figure 6 shows the Canberra Z error calculated for an experiment using the DSN plus the Spaceflight Tracking and Data Network (STDN) station in Hawaii. Figure 7 shows the Canberra Z error for a 4-station VLBI experiment including the former DSN station at Johannesburg, South Africa. Roughly speaking, the addition of a properly placed station to the DSN results in a sizeable improvement in the largest station location error component and a reduced need for low-elevation observations.

Figure 8 shows the effect of varying the thermal noise contribution to a VLBI experiment involving the three DSN stations and four radio stars at declinations of −0.5, 0, 0.17 and 0.8 radians. The noise contribution is indicated as number of bits recorded per station, although such variation can also result from varying source strengths. The point corresponding to the noise parameters of Eqs. (4) and (5), of 10^6 bits per observation, is shown for reference. Even if we assume optimistically that troposphere modeling errors are independent, we can operate with the total bit count in the neighborhood of 10^6 bits per observation, or 2×10^8 bits per total experiment—which fits on one computer tape—with little loss in resolution. If the assumption of independent troposphere errors is false, the thermal noise is still more strongly dominated by tropospheric effects; then, however, the desired 50-cm accuracy becomes unachievable. The truth should lie somewhere between these curves.

IV. Conclusions

Only a few conclusions arise naturally from the results presented here:

(1) Tropospheric modeling errors represent a dominant error source, which masks thermal receiver noise as long as enough data is recorded for detection.

(2) Independence between samples for the errors in the troposphere model is crucial to the delivery of meaningful results. If it is not achieved, then at least an order-of-magnitude improvement in model accuracy will be required.

(3) Observations on the Madrid–Canberra baseline are important when only the DSN stations are utilized.

V. Future Work

Several specific actions seem required to complete the analysis presented here:

(1) Add the capability to do directed observations as well as clock-driven observation sets.

(2) Add terms for ionospheric and other error sources.

(3) Experiment further with observations and weighting strategies.

These actions will be accomplished as time permits.

References

1. Williams, J. G., "Very Long Baseline Interferometry," JPL SPS 37-62, Vol. II, pp. 49–55, March 1970.

2. Madrid, G. A., et al., *Tracking System Analytical Calibration Activities for the MM'71 Mission*, JPL TR 32-1587, March 1974.

3. Hurd, W. J., "DSN Clock Synchronization by Maximum Likelihood VLBI," JPL TR 32-1526, Vol. X, DSN-PR, pp. 82–95, August 15, 1972.

4. Shapiro, I. I., *The Prediction of Ballistic Missile Trajectories from Radar Observations*, McGraw-Hill Book Co., New York, 1957.

5. Thomas, J. B., and Fanselow, J. L., *A Preliminary Covariance Analysis for the 14-63 Baseline*, IOM 3391.5-409, May 2, 1975 (JPL internal document).

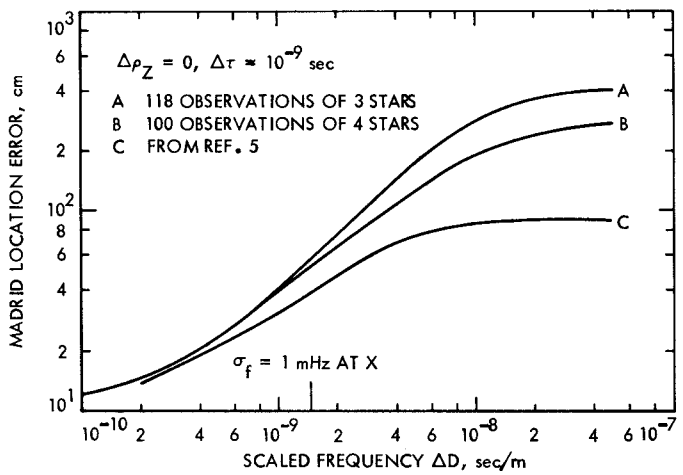

Fig. 1. Madrid location error vs. frequency error for fixed delay error, no troposphere

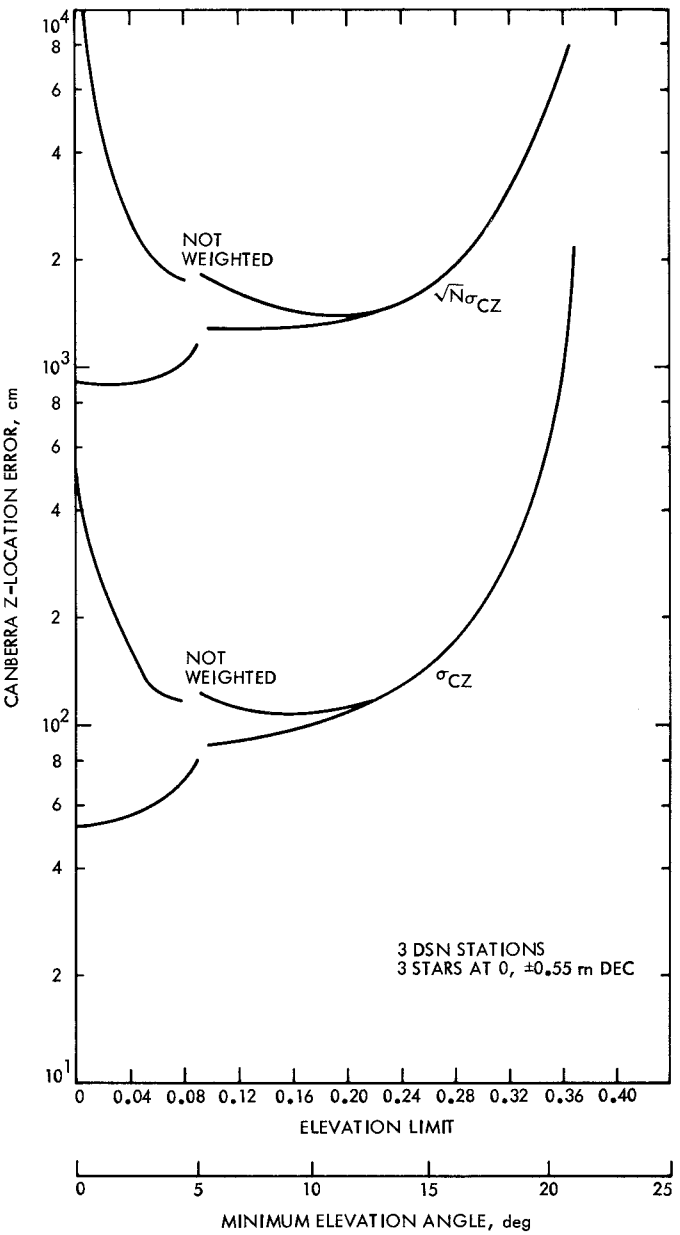

Fig. 2. Canberra location error vs. horizon with 3 DSN stations and 3 stars at 0 and ±0.55 rn

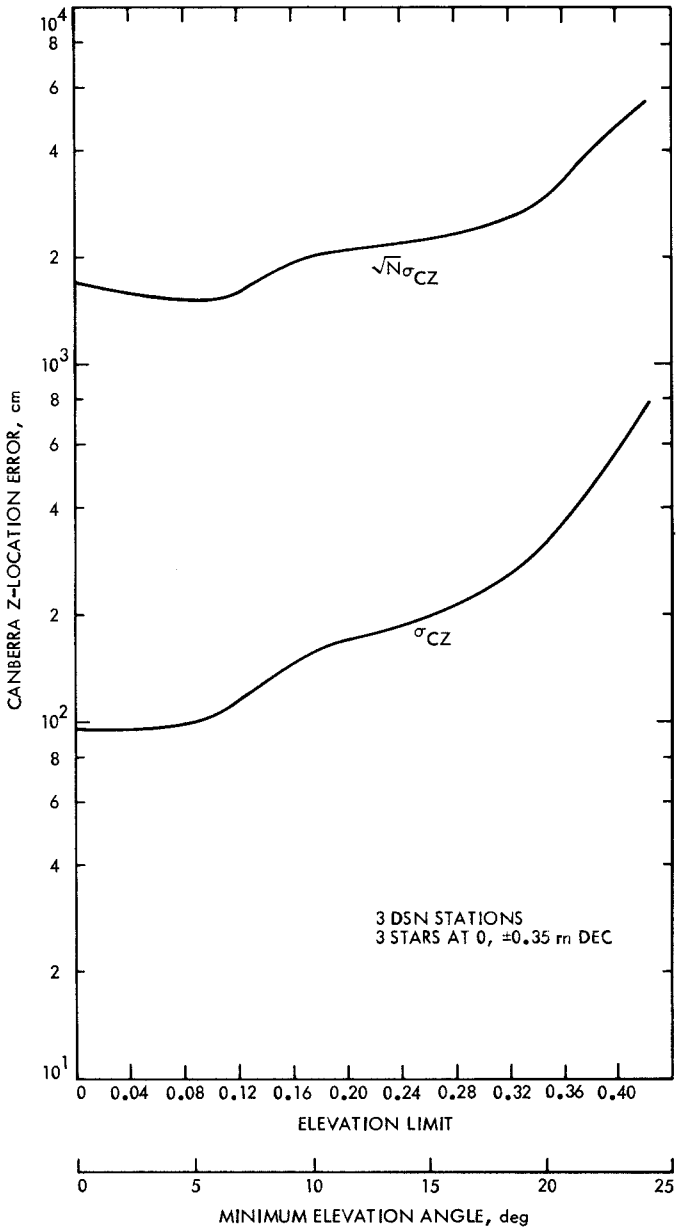

Fig. 3. Canberra location error vs. horizon with 3 DSN stations and 3 stars at 0 and ±0.35 rn

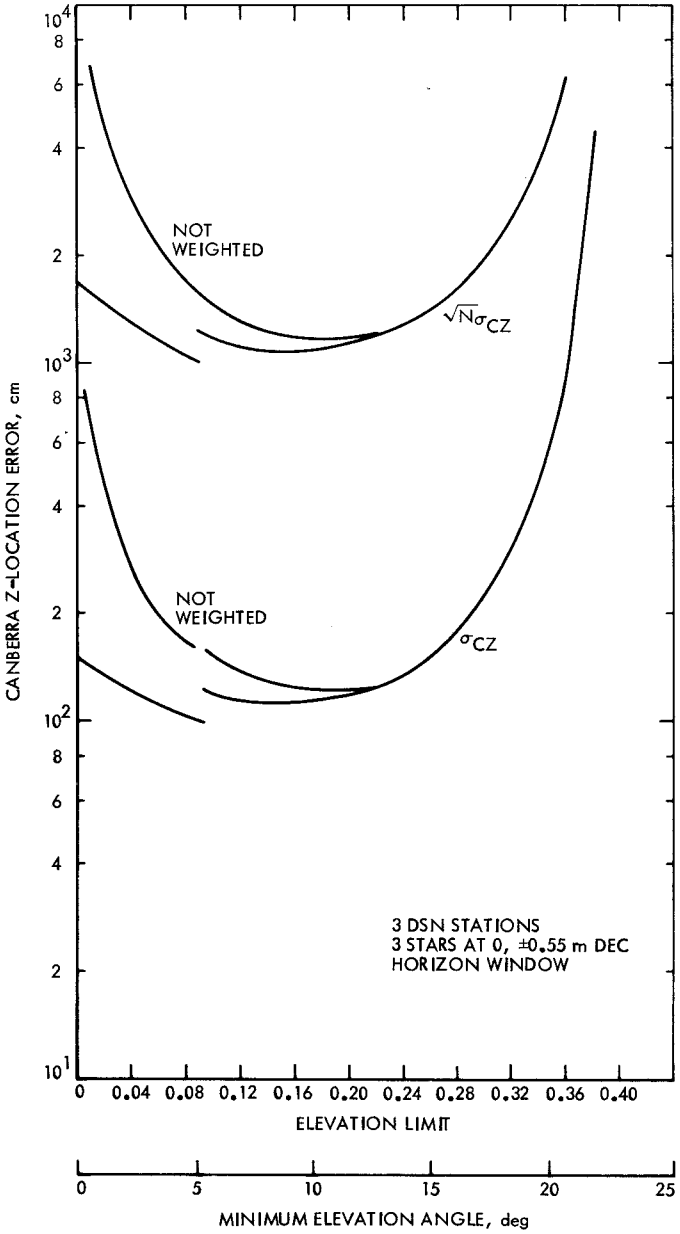

Fig. 4. Canberra location error with horizon window for 3 DSN stations and 3 stars

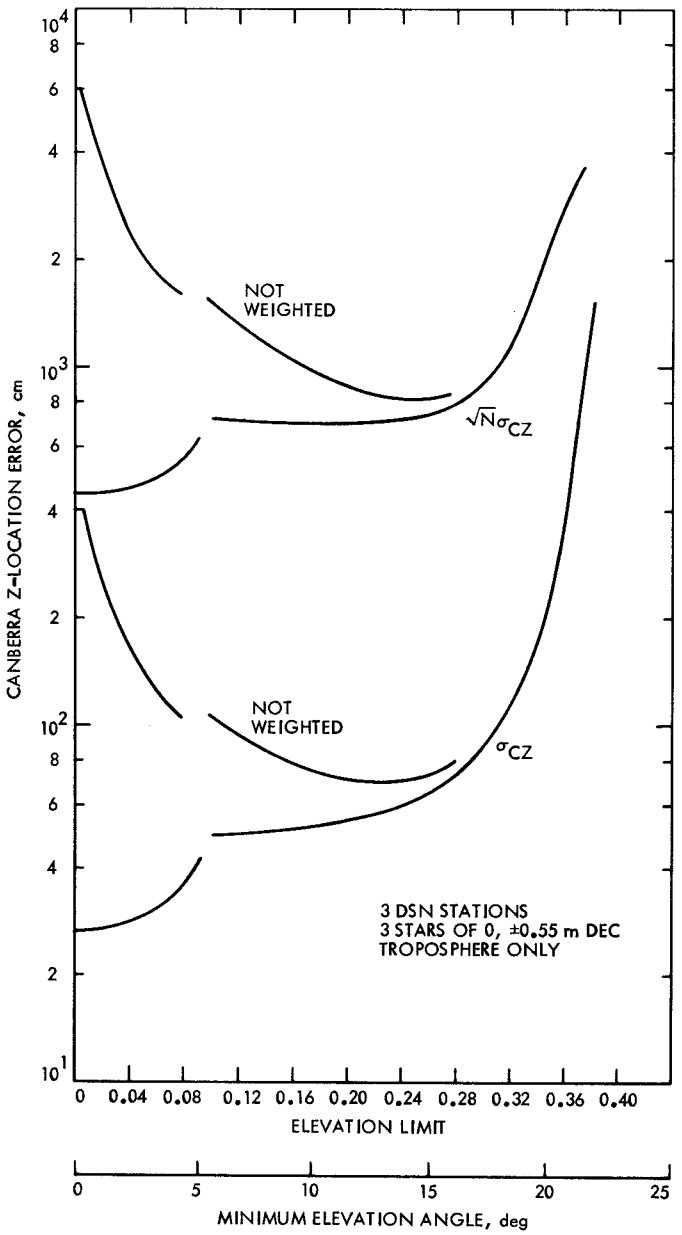

Fig. 5. Canberra location error vs. horizon for 3 DSN stations, 3 stars, troposphere noise only

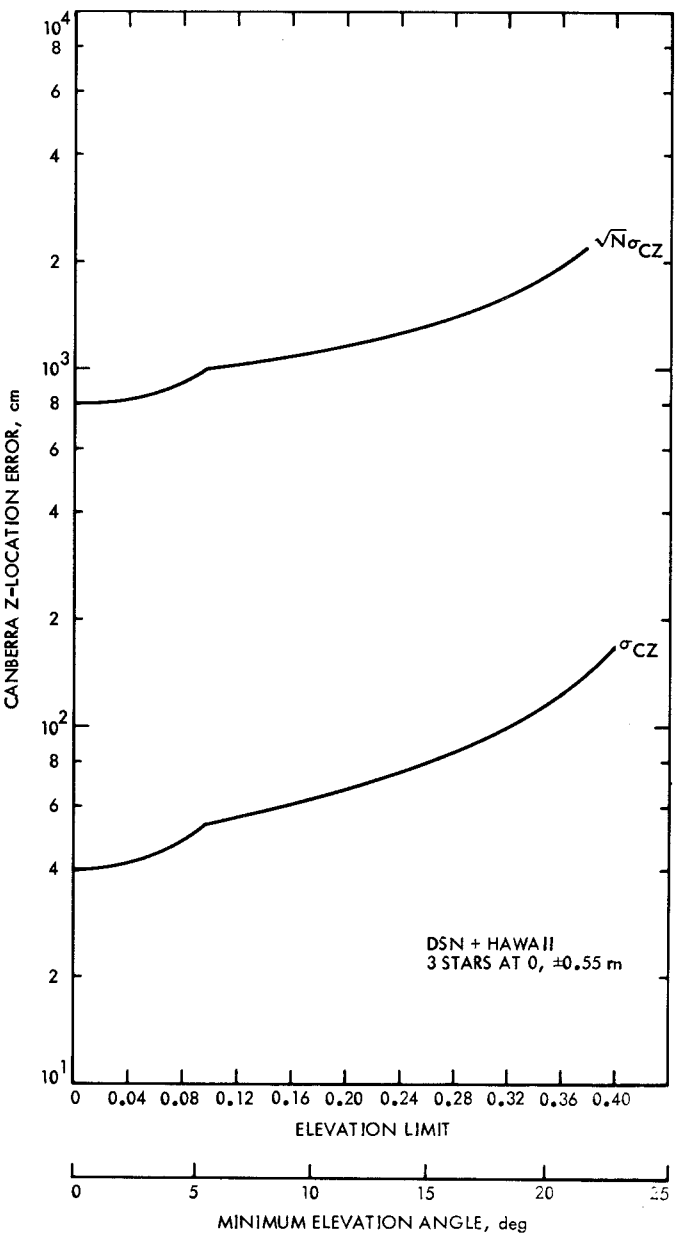

Fig. 6. Canberra location error for DSN plus Hawaii and 3 stars

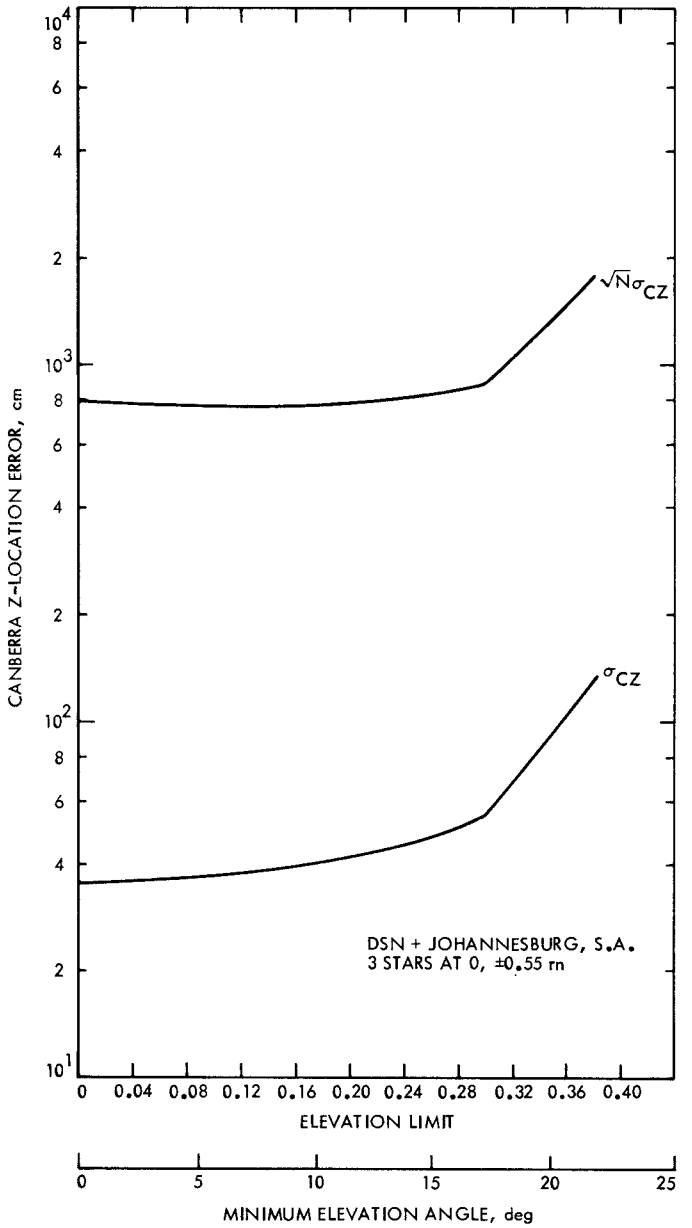

Fig. 7. Canberra location error for DSN plus Johannesburg, South Africa, and 3 stars

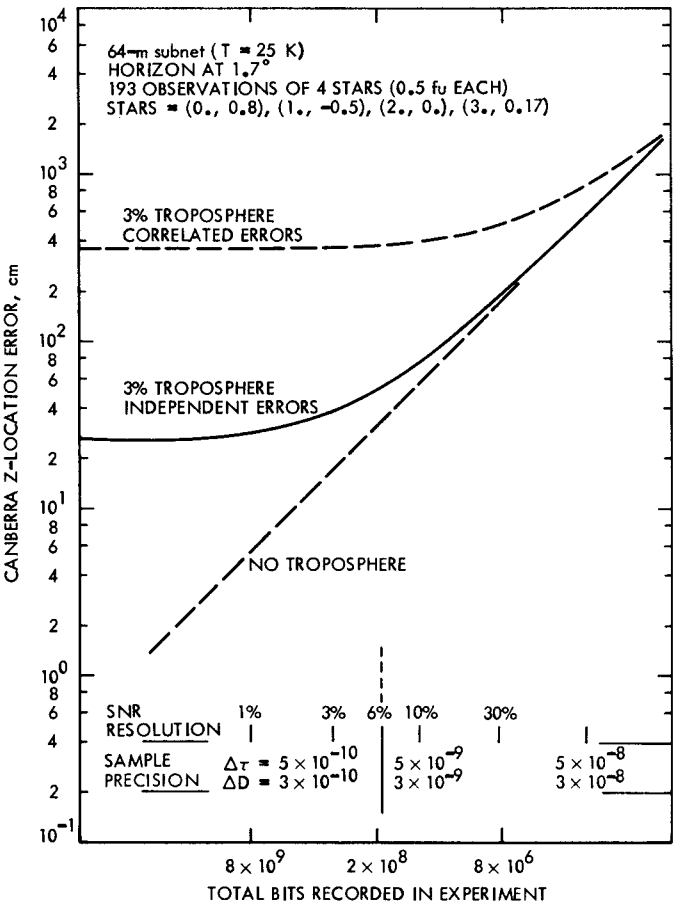

Fig. 8. Canberra location error vs. SNR for 3 DSN stations and 4 stars